Acta Technica *62* (2017), No. 6B, 1217–1234

Fast acquisition of building feature profile based on scanning point cloud

Xiaoling Sun[1,2], Jiping Hao[1], Qiang Xue[1,2], Chunlei Fan[1,2], Hanchao Liu[1,2], Mengnan He[1,2]

Abstract. The multi-core concrete-filled steel tube (MCFT) column which has the characteristic of large depth-to-width ratio of the cross-section is proposed in this paper. It is suitable for the residential buildings as a new type of composite column. To study the failure characteristic, hysteretic property,bearing capacity, deformability and energy dissipation capacity of these columns, a pseudo-static experiment was conducted for three full scaled specimens with depth-to-width ratio of 3.0 under high axial compression ratio. The results show that the specimens fail in an axial-flexural mode. The plastic area was located at the height of the bottom 1/3 section of the columns which was characterized by local buckling of steel plates, fracture of longitudinal welds of steel tube and crushing of concrete. The hysteretic curves of the columns are stable and haven't significant pinch phenomenon. The longitudinal partition can restrain the out-of-plane deformation of the steel plates effectively, thus increasing the buckling bearing capacity. As the columns fail, the displacement ductility coefficients are above 3.0 and the equivalent viscous damping coefficients are above 0.4 for all columns. Reducing the width-to-thickness ratios of the steel plates can effectively increase the energy dissipation capacity of the columns. When the design axial compression ratios vary from 0.54 to 0.68, the yield drift ratios of the columns are more than 0.005rad and the ultimate drift ratios are more than 0.02rad, showing excellent deformability and energy dissipation capacity. Furthermore, simplified formulas which are used to calculate the axial-flexural strength of the composite columns are proposed. The evaluated results show good agreement with the test results.

Key words. Multi-core concrete filled steel tube column, Bearing capacity, Axial compression ratio, Seismic behavior, Quasi-static test.

1. Introduction

At present, the assembled steel structure has been widely promoted in China because of its advantages of greenization and industrialization. In the assembled

[1]School of Civil Engineering, Xi'an University of Architecture & Technology, Xi'an 710055, China

[2]Design Institute of Xi'an University of Architecture & Technology, Xi'an 710055, China

steel structure, especially when the concrete filled rectangular steel tubular members are used in residential buildings, the frame column protrudes the wall and affects the building function. To properly increase the ratio of the aspect ratio of the section along the enclosure wall can reduce or even avoid the frame column from protruding the wall, and significantly improve the quality of steel structure residence [1]. At the same time, the flexural capacity and stiffness of the concrete filled rectangular steel tube surrounding the major axis strenghen with the increase of the aspect ratio of the section, which can effectively improve the force efficiency of the section, reduce the amount of steel and reduce the cost.

Scholars at home and abroad have made a great deal of research and improvement on concrete filled rectangular steel tubular members [2∼6]. Huang Hong and other researchers [4] have researched mechanical behavior of axially compressed concrete filled steel tubular stub columns with ribs, and set stiffeners to increase the longitudinal stresses of core concrete, reduce tensile stress range of steel pipe wall, and improve the stability of the wall. Cai Jian and other researchers [5] have researched axial bearing capacity of concrete filled rectangular steel tube with binding bars, which is helpful to delay the local buckling of steel tubes, improve the axial bearing capacity and ductility of concrete filled rectangular steel tubular short columnn. Guo Lanhui and other researchers [6] have studied on mechanical behavior of thin-walled concrete filled rectangular steel tubular members with stiffener and section aspect ratio of 2.4, finding that stiffened thin-walled plates can change the buckling mode of the steel plate, and improve the buckling bearing capacity of the plate. In the past, theoretical analysis and testal research mainly refer to concrete filled rectangular steel tube concrete or concrete filled square steel tube with small aspect ratio of the section, which was generally less than 2.0.

This paper presents a new type of multi-core concrete filled steel tube column (MCFT Column, hereinafter referred to as multi-core column) suitable for steel structure residence; the typical column section is as shown in Fig. 1. In order to reduce the width-to-thickness ratio of steel plate of long side of section, and form an effective constraint on the concrete, a wide flange I-shaped cross-section is formed by welding the steel tube web with the clapboard, and then flange plate or rectangular steel tube is welded on both sides, forming two-core or multi-core concrete filled steel tube columnn. The form of the section can make full use of existing I-shaped and box section production lines and reduce the technological difficulty. A multi-core column with a cross-section aspect ratio of 3.0 is adopted in a steel residential building in Xi'an, the seismic performance and design method of this kind of member are not given in the existing research and specifications [7–9]. Therefore, in this paper, the frame columns of this residence is taken as a model, and low-cycled reversed loading testunder high axial compression ratio on the multi-core column full-scale specimen with cross-section aspect ratio of 3.0 is carried out to study the failure mode, bearing capacity, deformation capacity and energy dissipation capacity, etc, in this paper, the effects of axial compression ratio and steel ratio on seismic performance of multi-core columns are discussed, and normal section bearing capacity calculation formula is proposed, which provides a reference for the engineering application of the new multi-core column.

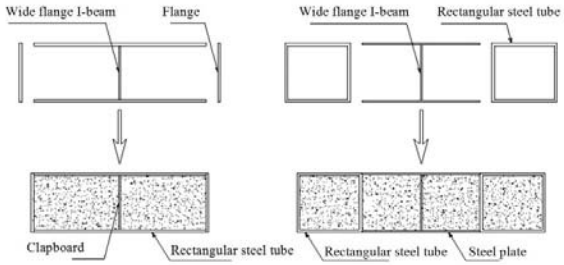

Fig. 1. Section of MCFT column

2. Introduction of test

2.1. Specimen design

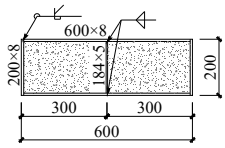

(a) Sectional drawing of specimens C1∼C2

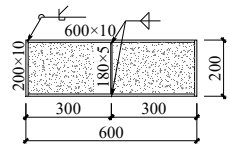

(b) Sectional drawing of specimen C3

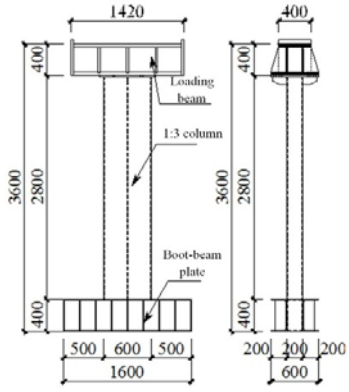

(c) Specimen elevation

Fig. 2. Dimensions and details of specimens

In this test, a concrete filled rectangular steel tubular column in a residential engineering in Xi'an is selected. The specimen section size is 200mm × 600mm, and the height is 3600mm. The specimen is arranged at the bottom of welded steel structure boot-beam plate and column and is arranged on the top of high-strength bolts connection of steel structure loading beam and column. The width-to-thickness ratio of the web of specimen C1∼C3 exceeds the limit specified in Technical Specification for Structures with Concrete-Filled Rectangular Steel Tube Members (CECS159:2004), in order to prevent premature occurrence of local buckling before the steel tube reaches ultimate bearing capacity, separate steel plate with thickness

of 5mm is arranged in the middle of the steel tube web, which is as shown in Fig. 2.

The average cube compressive strength of concrete is measured 32.3MPa in the test, and the standard value is 28.1MPa. Both steel tube and steel plate are made of Q235B grade steel. The measured values of yield strength and tensile strength are shown in Table 1, and the boot-beam plate and the loading beam are made of Q345B grade steel.

Table 1. Mechanical properties of steel

/mm	/mm	$f$sm /MPa	$f$su /MPa	E /MPa	δ /%
5	4.60	318.5	475.2	2.05×105	40.1
8	7.68	317.9	481.9	2.08×105	40.1
10	9.67	315.4	454.4	2.06×105	27.5
Note: $f$sm is yield strength; $f$su is tensile strength; E is elastic modulus; δ is elongation					
Nominal thickness /mm	Measured thickness /mm	$f$sm /MPa	$f$su /MPa	E /MPa	δ /%
5	4.60	318.5	475.2	2.05×105	40.1
8	7.68	317.9	481.9	2.08×105	40.1
10	9.67	315.4	454.4	2.06×105	27.5

2.2. Testal parameter

The major variation parameters of the specimen are axial compression ratio and steel ratio.

The design value nd and testal value nt of axial pressure and axial compression ratio of each specimen are shown in Table 2. When the axial compression ratio is calculated, the effect of steel tube is considered, and the design value and testal value are calculated using formula (1) $\sim$ (2):

$$n_d = 1.2N/\left(f_s A_s + f_c A_c\right) . \tag{1}$$

$$n_t = N/\left(f_{sm} A_s + f_{cm} A_c\right) . \tag{2}$$

In the formula, N is the axial pressure of column; fs is design value of yield strength of steel; $f$sm is measured value of yield strength of steel; As is steel tube section area, in which the longitudinal separation plate functions as structuring, effect of which is not considered in axial compression ratio and bearing capacity calculation; fc is the design value of the axial compressive strength of concrete; $f$cm is the axial compressive strength of concrete, $f$cm=0.76$f$cu, $f$cu is the measured value of cube compressive strength of concrete; Ac is net sectional area of concret.The parameters setting of steel pipe and steel plate are shown in Table 2. The specimens meet the limit requirements for the width-to-thickness ratio of concrete filled rectangular steel tube specified in the Technical Specification for Structures with Concrete-Filled Rectangular Steel Tube Members (CECS159:2004). The steel ratio is the ratio of the steel section area to the column section area. The steel ratios of

the specimens are 10.04% and 12.58% respectively.

Table 2. Main test parameters

Specimen No.	Axial compression load N/kN	Axial compression ratio		Width-to-thickness ratio		Steel ratio
		nd	nt	Flange	Web	
C1	2196.5	0.68	0.34	23.0	36.5	10.04%
C2	1757.2	0.54	0.27	23.0	36.5	10.04%
C3	2196.5	0.59	0.30	18.0	29.0	12.58%

2.3. Test equipment, measurement items and loading system

The test is a pseudo static test of repeated horizontal loading under constant axial compressive load. The test device is shown in Fig. 3. As regulated in JGJ/T 101-2015 Code for Seismic Test of Buildings [10], force-displacement hybrid control mode of loading is adopted. Firstly, the vertical jack applies axial load, and in the test process, axial compression load stays unchanged through the pressure stabilizing system; secondly, the servo actuator applies repeated horizontal load, the distance between horizontal force loading point and column bottom section is 3000mm, and the distance between main control point displacement meter D1 and column bottom section is 2600mm, which is as shown in Fig. 4. The horizontal load of the specimen is controlled by force control before the yield load is predicted, the loading level is 0.2 times the predicted yield load, and each load is cycled for once; after yielding of the specimen, control the loading according to the displacement, the displacement increment of corresponding main control points of each load level is 10mm, with 3 cycles for per level displacement. At the horizontal loading, thrust is applied first as the forward loading, and tension is applied secondly as the reverse loading. The test stops when the specimen fails to maintain the applied axial pressure or horizontal load due to the buckling of the steel plate and the concrete crushing, and dropped to less than 85% of the peak horizontal force.

The test measurements include the applied axial compression load and horizontal load, the displacement of the specimen and the strain at critical location. The arrangement of measuring points is as shown in Fig. 4, along the column height, 5 horizontal displacement measurement are arranged to measure horizontal displacement, at the bottom of the column, 1 pair of cross displacement measurement is arranged to measure shear deformation of specimen; at the ground beam, 3 displacement meters are arranged to monitor horizontal sliding and rotation of boot-beam plate; the lower part of the column is arranged 2 inclinometers to measure column section rotation angle. In addition, strain rosettes are placed at the places 200mm and 550mm apart from the bottom of the column to measure the longitudinal strain, circumferential strain and shear strain of the steel tube at the bottom of the column. During the test, the development of the buckling of the steel plate and the damage of the welding seam are observed and recorded.

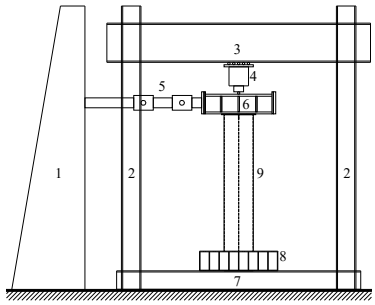

1. Reaction wall;2. Reaction rigid frame;3. Reaction beam;4. Jack;
5. Servo actuator;6. Loading beam; 7. Pedestal;8. Boot-beam plate;9. Specimen

Fig. 3. Test setup

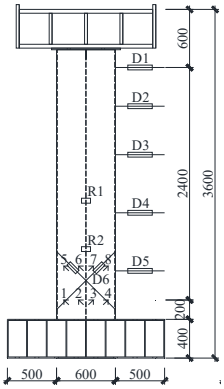

D1. Magnetostrictive displacement meter;D2∼D5. Horizontal displacement meter;
D6. Cross displacement meter;R1∼R2. Inclinometer;1∼8. Strain rosette

Fig. 4. Measuring points distribution of specimens

3. Test results and analysis

3.1. Failure process and failure modes

The failure process and failure modes of the 3 specimens are basically the same, and the test process can be divided into the following 3 stages:

1) Elastic stage. At the initial stage of loading, each specimen deformation is small, before the specimen nominal yield (displacement is about 15mm, the displacement angle is about 0.006 rad, specimens vary), it is basically in the elastic state with small residual deformation and without the occurrence of local buckling of steel tube.

2) Elastic-plastic stage. This stage is the loading process after the nominal yield reaches the peak value of the horizontal load. When the displacement reaches 20mm (displacement angle is about 0.0075 rad), there is local micro buckling at the bottom rectangular steel tube of specimens C1 and C2 arising from compression flange,

the tension end occurs micro sag. As the displacement increases, rectangular steel tube compression web occurs micro buckling. In the loading process, the compressive deformation of concrete under compression flange position is maximum, due to Poisson effect, there is transverse expansion, resulting in steel flange buckling earlier than that in web. When the displacement reaches 40mm (displacement angle is about 0.015 rad), there is compression steel plate buckling and slight expansion at the bottom rectangular steel tube of specimens C1 and C2, and there is buckling of flange and web of the compression zone at the bottom of the specimen C3, since the buckling is slight and there is no obvious buckling order. At this time, the horizontal load of each specimen reaches its maximum value.

3) Failure stage. At this stage, when the horizontal load reaches the peak, the specimen appears larger plastic deformation, and the horizontal load begins to decrease until below 85% of the peak load or lose the vertical bearing capacity. When the displacement is more than 50mm (displacement angle is about 0.020 rad), there is obvious buckling of steel plate of the rectangular steel tube compression zone at the bottom of specimen, and the buckling of the steel plate in tension zone cannot be straightened. The buckling concentrates on the range from 1/3 column section height to the bottom. Because the web width-to-thickness ratio is greater than the flange width-to-thickness ratio, the buckling of web develops faster than that in flange. Specimen C1 is of maximum axial compression ratio, so the buckling phenomenon is the most obvious, and residual tensile zone deformation is at maximum. The buckling of steel plate and residual deformation of specimen C2 is relatively small than specimen C1. The axial pressure of specimen C3 is relatively small, the thickness of the steel plate is large, the buckling development of its steel plate is slowly. When the displacement reaches 60mm (displacement angle is about 0.025 rad), there are vertical cracks at the corner welding of compression zone of specimen C1 steel tube, residual buckling and deformation increase significantly. Buckling and residual deformation of compression zone of rectangular steel tube of specimens C2 and C3 specimens further develop. When the displacement reaches 70mm (displacement angle is about 0.030 rad), vertical cracks of rectangular steel tube of specimen C1,and the internal concrete chips off rapidly, the horizontal bearing capacity drops sharply, at the end of the test; buckling of rectangular steel tube siding of specimens C2 and C3 continues to develop with the scope expanded. When the displacement reaches 80mm, the welds of the corner steel pipe at the bottom of the column of specimens C2 and C3 cracks, the internal concrete chips off, the horizontal bearing capacity drops rapidly, and the test is finished. The specimens can keep the axial force unchanged during the whole loading process, and the vertical bearing capacity does not appear obvious decline.

The overall failure mode of the specimen is shown in Fig. 5. The specimens C1 and C2 form a bent plastic zone at a distance of about 200mm from the bottom of the column, and the specimen C3 forms a bent plastic zone at a distance of about 250mm from the bottom of the column. Each specimen shows obvious residual buckling deformation at flanges and webs of steel tube at the bottom, the central part of the specimens are restricted effectively by clapboard, the web is divided into two buckling half wave. Although there is serious buckling of steel plate in the late

(a) C1 Specimen C1 (b) C2 Specimen C2 (c) C3 Specimen C3

Fig. 5. Failure mode of specimens

period of loading, the concrete has far exceeded the compressive peak strain, due to steel tube and clapboard form an effective horizontal constraint on the concrete, and effective compression area of concrete increases after buckling of steel tube, the macro horizontal bearing capacity of specimens has not decreased significantly. With the increase of the horizontal displacement of the specimens, the expansion stress of the concrete increases, and the cumulative damage of the welds occurs under the action of the reciprocating load, and the corner welds of the steel tube flanges are all cracked. The specimen C3 steel tube has the strongest confinement to concrete while expansion stress of the concrete is the maximum. When the steel tube welds crack, the speed is fast and the noise is loud, and the length of the weld tear is large. After the cracking of the steel tube welds, the concrete loses its horizontal restraint, mutual restraint between steel plates disappears, and the horizontal bearing capacity of the specimen drops rapidly.

Fig. 6 shows the failure mode of steel plate and concrete details of specimens, in the non plastic zone, the steel plate is well bonded to the concrete without obvious relative slip; concrete failure location is concentrated, near the position of flange, concert is crushed under cyclic loading, there is only a small amount of concrete cracks in the upper and lower regions of the plastic zone; there is buckling of steel tube siding at the plastic zone, the longitudinal baffle can effectively restrain the buckling of steel plate plane, which forms horizontal residual deformation under the expansion force; the I-shaped section formed by the clapboard and the adjacent web has significant binding effect on the concrete, forming central "compressed core zone", ensuring vertical bearing capacity of the specimen in the whole process.

3.2. Hysteretic curve and skeleton curve

Fig.7 is the load-displacement hysteretic curve of specimens C1∼C3. The ratio of shear deformation of the specimen to the horizontal displacement of the main control point is less than 10% by measuring the cross displacement. It shows that the deformation of the specimen is mainly dominated by bending deformation.

As can be seen from Fig.7: 1) at the initial stage of loading, the specimen is in an elastic state. When the horizontal displacement is less than 15mm, the hysteretic curve is basically linear, and the residual deformation is small. When the displacement is greater than 15mm, the steel yield, the stiffness decrease, the load increases

(a) Weld tear of steel tube

(b) Horizontal residual deformation of clap-board

(c) Concrete crushing at the bottom of column

Compressed core zone

Fig. 6. Failure mode of steel plate and concrete

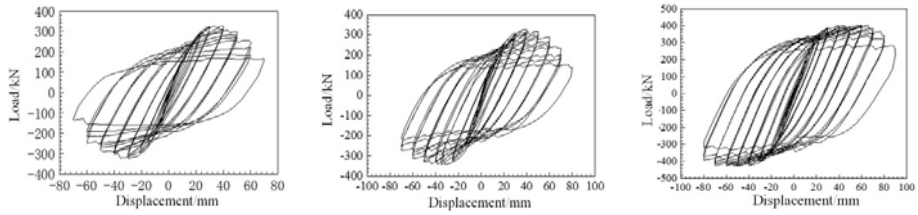

(a) C1 Specimen C1 (b) C2 Specimen C2 (c) C3 Specimen C3

Fig. 7. Hysteretic curves of specimens

steadily, and the residual deformation occurs after unloading. When the horizontal displacement is 40mm, the load reaches its peak value, there is buckling of steel plate, the residual deformation is obvious, and the surrounding area of hysteresis loop increases, and the cumulative loss of energy increases. When the loading is continued, the bearing capacity and stiffness of the specimen are obviously reduced, and the residual deformation increases significantly. 2) Under the same displacement, the area enclosed by the hysteresis loop decreases gradually with the increase of the number of loading cycles. It shows that the specimen has accumulated damage and the energy dissipation capacity becomes weak. 3) The hysteresis curve of each specimen is full, and there is no obvious pinch phenomenon, showing good seismic performance. 4) the smaller the axial compression ratio of the specimen, the more slowly the load decreases in the later stage of loading, and the more energy accumulated and dissipated, the stronger the deformation capacity. With the increase of the steel ratio, the width-to-thickness ratio of the steel plate decreases, and the energy dissipation capacity and deformation capacity of the specimens increase obviously.

The skeleton curve can reflect the change of rigidity, bearing capacity and ductility of the specimen in the whole process. The skeleton curves of each specimen are S-shaped and basically origin-symmetric, as shown in Fig. 8. It can be seen from the figure that: 1) at the initial stage of loading, the skeleton curves of each specimen coincide basically, and the initial stiffness is basically the same. With the increase of displacement, the specimens steel yield, the steel plate appears buckling successively, and the skeleton curve begins to appear different. 2) when the peak value of horizontal load is reached, the bearing capacity of specimens C1 and C2 is basically the same, and the wall thickness of steel tube of specimen C3 is large

and the bearing capacity is the highest. 3) After reaching the horizontal peak load, skeleton curve of specimens C1 and C2 begins to enter the descending section, axial pressure of specimen C2 is small and the decline is more flat, width-to-thickness ratio of steel tube of specimen C3 is small, and axial compression ratio is also small, local buckling of steel plate occurs later, constraints on the concrete of steel pipe is strong, the bearing capacity after the specimen yields remains unchanged in plastic flow state.

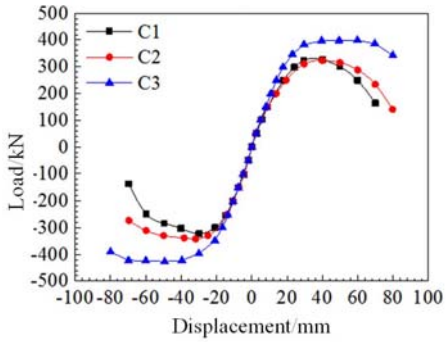

Fig. 8. Skeleton curves of specimens

3.3. Bearing capacity and deformability

Multi-core column load-displacement skeleton curve has no obvious yield points and the failure points, the nominal yield load is determined by the following methods [11]: the nominal yield displacement refers to the displacement between the extension line of the elastic section of the skeleton curve and the point of intersection of tangent at the peak point, the corresponding load is the nominal yield load; limit displacement is the displacement when the horizontal load when the specimen falls to 0.85 times the peak load.

The load, displacement and interlayer displacement angle at each stage are shown in Table 3. As shown in Table 3, the nominal yield load of each specimen is about 0.75 times of the peak load. The yield and ultimate bearing capacity of specimens C1 and C2 are close to each other, and the bearing capacity of specimens C3 is higher. Specimen C3 has the same axial pressure as specimen C1, but the steel ratio of C3 increases by 28.9% than C1, and the peak load increases by about 22% compared with that of C1. The specimens C1∼C3 can meet the requirements of the limit of 1/50 of elastoplastic interlayer displacement angle of multilayer and high-rise concrete filled rectangular steel tubular structures in China. The axial compression ratio of specimen C2 is 26% lower than that of C1, the ultimate deformation increases by about 15%, but the ultimate deformation increases greatly by about 47.4%. This is because the increase of steel ratio can reduce the axial compression ratio of specimens, with the decrease of width-to-thickness ratio of steel plate, the plastic bearing capacity can be more effective, at the same time, steel tubes provide stronger horizontal restraints on concrete, which can improve the brittleness mechanical behavior

of concrete, so that the specimen has better deformation ability in the macroscopic aspect.

3.4. Ductility and energy dissipation capacity

The displacement ductility coefficient μ of the specimen is calculated according to yield displacement Δ_y and limit displacement Δ_u in Table 3:

$$\mu = \frac{\Delta_u}{\Delta_y}\,. \tag{3}$$

The energy dissipation capacity of the specimen is measured in terms of the area enclosed by the load-displacement hysteresis curve, the equivalent viscous damping coefficient ζeq and the accumulative energy dissipation can be adopted for assessment. The ζeq is calculated according to the area enclosed by the curve ABCD and areas of triangles OBE and OBF in Fig. 9:

$$\zeta_{eq} = \frac{1}{2\pi}\frac{S_{(ABC+CDA)}}{S_{(OBE+ODF)}}\,. \tag{4}$$

The results of the ductility coefficient calculated based on formula (3), the ζeq,p under forward and reverse loading of the cycle of peak load point calculated based on formula (4), and the last stage of cyclic loading ζeq,u are shown in Table 4. The accumulative energy dissipation of each specimen is shown in Fig.10. The results show that: multi-core column has good deformation capacity, and its ductility coefficient is greater than 3.0; the smaller the axial compression ratio, the higher the steel ratio, and the better the ductility; specimens C1 $\sim$ C3 equivalent viscous damping coefficients are all greater than 0.4, which have a strong energy dissipation capacity; specimen C3 gives full play to the steel plasticity and can dispatch more energy, the accumulative dissipated energy is about 2 times the specimen C1.

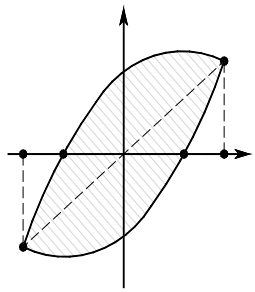

Fig. 9. Calculation of equivalent viscous damping coefficients

Table 3. Main test results

θy/rad	Vp/kN	Δp/mm	θp/rad	Vu/kN	Δu/mm	θu/rad
0.0066	326.1	39.9	0.0153	277.2	55.0	0.0212
0.0061	322.3	29.9	0.0115	274.0	54.2	0.0208
0.0062	323.8	39.9	0.0153	275.2	62.9	0.0242
0.0060	341.8	34.8	0.0134	290.6	65.6	0.0252
0.0077	399.0	39.6	0.0152	342.6	79.9	0.0307
0.0080	426.9	49.3	0.0190	390.5*	80.0	0.0308

Table 4. Ductility and equivalent viscous damping coefficients of specimens

Specimen No.	Loading direction	Yield			Peak			Failure		
		Vy/kN	Δy/mm	θy/rad	Vp/kN	Δp/mm	θp/rad	Vu/kN	Δu/mm	θu/rad
C1	Forward	242.4	17.2	0.0066	326.1	39.9	0.0153	277.2	55.0	0.0212
	Reverse	264.8	15.9	0.0061	322.3	29.9	0.0115	274.0	54.2	0.0208
C2	Forward	222.5	16.2	0.0062	323.8	39.9	0.0153	275.2	62.9	0.0242
	Reverse	265.8	15.6	0.0060	341.8	34.8	0.0134	290.6	65.6	0.0252
C3	Forward	320.1	19.9	0.0077	399.0	39.6	0.0152	342.6	79.9	0.0307
	Reverse	346.8	20.7	0.0080	426.9	49.3	0.0190	390.5*	80.0	0.0308

Note: Vy, Vp and Vu are respectively nominal yield load, peak load and failure load; Δ_y, Δ_p and Δ_u are respectively displacement of nominal yield load, peak load and failure load; θ_y, θ_p and θ_u are respectively interlayer displacement angles of θ_y, θ_p and θ_u, $\theta = \Delta/H$, H is the height from the measured point to the bottom of the column; in the forward loading, the steel tube cracks and the reverse does not continue to load, and the load does not fall to 85% of the peak load.

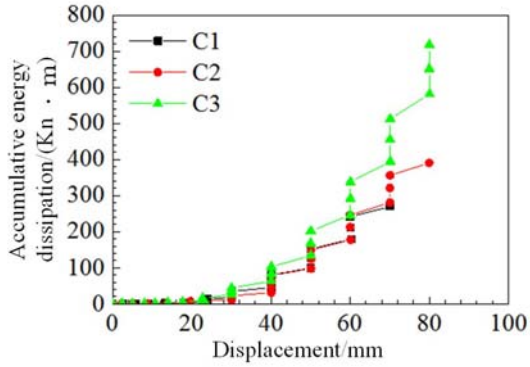

Fig. 10. Energy dissipation curves of specimens

3.5. Stiffness degradation

The stiffness degradation can reflect the effects of accumulative damage of component, secant stiffness can be used to characterize the stiffness degradation of the

specimen during loading, its value is the average value of the ratio of the peak load and the corresponding displacement at each stage under the same displacement. The stiffness degradation curves of each specimen are shown in Fig. 11. It can be seen from the Figure that, the secant stiffness of each specimen degenerates rapidly after entering the elastic-plastic stage. With the plastic development of the steel, the stiffness degradation tends to be gradual. The positive stiffness of the specimen is smaller than the negative stiffness, it is because the steel is strengthened during forward loading, and the specimen has higher bearing capacity during reverse loading. The stiffness of the member with relatively small axial load is reduced more slowly, and the increase of the steel ratio can effectively improve the secant stiffness of the specimen and make the specimen exhibit better seismic performance.

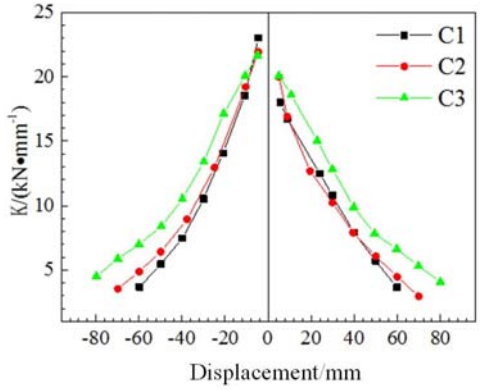

Fig. 11. Stiffness degradation curves of specimens

3.6. Strain of steel at the bottom of column

Fig. 12 is the horizontal load-vertical strain hysteretic curve at flange position at the bottom of the specimen. When the horizontal load reaches the nominal yield load of the specimen, the steel begins to yield and the compressive strain is slightly larger than the tensile strain. When the horizontal load reaches the ultimate bearing capacity of the specimen, the surface strain of the steel tube has exceeded the yield strain. Continue to increase the horizontal displacement, steel plate buckling begins to develop, concrete gradually lose its restraint, and the steel compressive strain develops rapidly. After that, the concrete is crushed and the compressive stress of the specimen is transferred to the steel tube. The strain curve of the steel is divergent and no tensile strain occurs. The specimen C1 quickly loses bearing capacity after the strain divergence; C2 also gradually lose the bearing capacity after compression strain experiences many cycles; buckling of steel plate of specimen C3 develops slowly, in the late loading, it can basically complete the tension and compression strain cycling, showing good deformability.

Fig. 13 shows the strain distribution of vertical strain of plastic section at bottom of column along the column section. It can be known from the Figure that, in case

of the nominal yield load, the strain distribution of section accords with the plane section assumption; when the horizontal force reaches peak load, because the uneven distribution and development of steel buckling, the strain distribution deviates from the straight line, but basically accords with the plain section assumption.

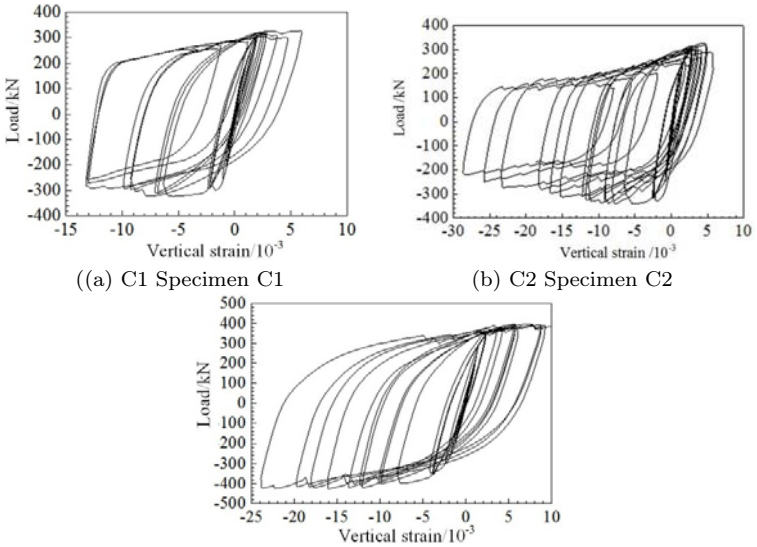

((a) C1 Specimen C1 (b) C2 Specimen C2

(c) C3 Specimen C3

Fig. 12. Hysteretic curves of lateral force versus plate's vertical strain of specimens

4. Calculation of bearing capacity

The failure locations of the specimens are concentrated around the area with distance of 200-250mm from the bottom of the column, and form a typical column bending plastic hinge. When the peak load is reached, the strain distribution is basically consistent with the plane cross-section assumption. Therefore, the horizontal bearing capacity can be calculated by the compression-bending capacity of normal section of bottom section of MCFC column. When the calculation of normal section bearing capacity in this paper, the full cross-section plastic method is adopted, and the following assumptions shall be used, including the synergistic effect between steel tube and concrete, and that the deformation accords with the plane section; the effect of tensile concrete is not considered; the concrete in compressive zone is calculated based on the equivalent rectangular stress block. In the limit state, the stress and strain distributions of the section of MCFT column are shown in Fig.14.

When the ratio of width to thickness of concrete-filled rectangular steel tubular (CFST) is $R<0.85$[12], the steel plate can reach the yield strength, but it is prone to local buckling. The average stress of steel plate hardly exceeds the yield strength. The web of steel tube is in the bend shear and complex mechanical state, but the shear stress does not exceed 0.5 times of the shear strength of the web. The reduction

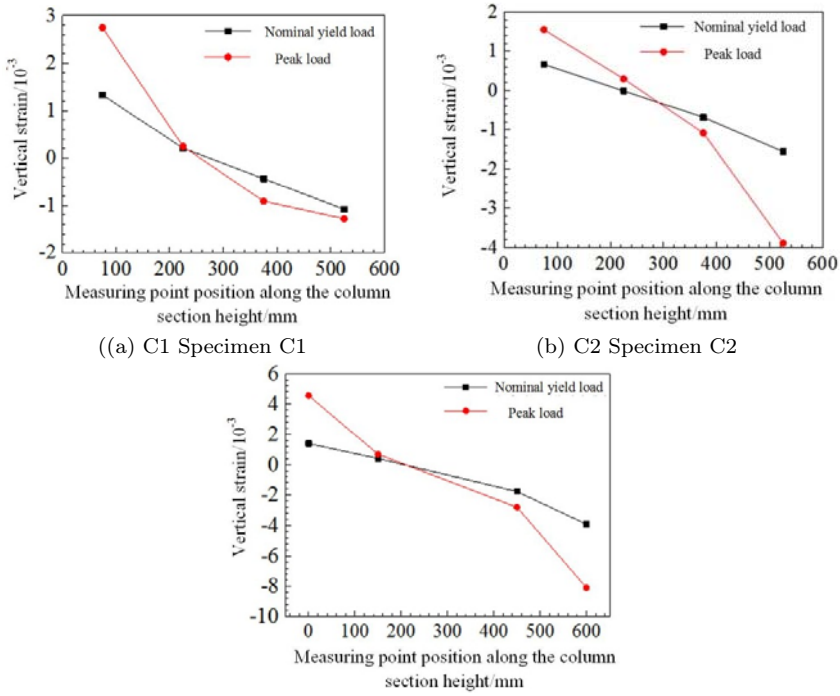

((a) C1 Specimen C1 (b) C2 Specimen C2

(c) C3 Specimen C3

Fig. 13. Vertical strain distribution of bottom section of specimens

of shear stress on bending strength can be neglected. Therefore, the yield strength is used for the strength of steel tubes.

The interaction mechanism between steel tube and concrete of MCFT column is very complicated. In the ultimate state, the force of concrete is similar to that confined by stirrup, and the steel tube and partition can be regarded as stirrups continuously distributed. After a large number of trial calculations, the transverse restraint stress of concrete could be obtained by referring to the literatures [13 and 14], and then the strength of concrete under the constraint of steel tube can be obtained from the Leon-Pramono criterion [14].

The location of plastic neutral axis could be determined based on the following formula:

$$N = f_{sm}A_{sw0} + f_{ccm}A_{cc}\,. \tag{5}$$

The bending capacity of specimen is calculated based on the following formula:

$$M_{u,N} = f_{sm}A_{sf}h_{sf} + f_{sm}A_{sw}h_{sw} + f_{ccm}A_{cc}h_c\,. \tag{6}$$

Under the consideration of $P-\Delta$ effect, the horizontal bearing capacity of MCFT column is:

$$V_{pe} = \frac{M_{u,N}\,.N\Delta_p}{H} \tag{7}$$

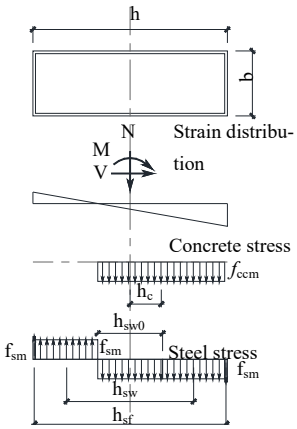

Fig. 14. Axial-flexure strength evaluation of column section

Where: N is the axial pressure; $f$sm and $f$ccm respectively present steel yield strength and axial compressive strength of confined concrete; Asw0 is the central area of web pressed; Asw and Asf respectively present areas of web bent and flange; $h$sw and $h$sf respectively present corresponding lengths of actuating arms of web bent and flange; Acc is the area of concrete under compression; hc is the distance of resultant force of concrete in compressive zone from the column cross-section center; Δp is the top displacement corresponding to peak load; $H$is the distance of loading point from the bottom of column.

Table 5 presents the horizontal ultimate bearing capacity of the specimens, and gives the ratio of the experimental peak value to the calculated value. The calculation results show that the calculated value of horizontal ultimate bearing capacity agrees well with the positive test value, and the error is less than 10%.

Table 5. Measured peak load and calculated strength of specimens

Specimen No.	Loading direction	Trial value/kN	Calculated value/kN	Trial value/calculated value
C1	Positive	326.1	305.1	1.07
	Negative	322.3		1.06
C2	Positive	323.8	310.0	1.04
	Negative	341.8		1.10
C3	Positive	399.0	376.4	1.06
	Negative	426.9		1.13

5. Conclusions

The conclusions are got by low-cycled reversed loading test under high axial compression ratio on the multi-core column full-scale specimen with cross-section aspect ratio of 3.0:

1) The failure mode of the multi-core column is of failure by bending, in which the plastic zone is located at 1/3 of the depth section of the bottom column where the steel plate is compressed so that it protrudes and bends, the longitudinal weld of the steel tube is cracked and the concrete is crushed.

2) The hysteretic curves of the multi-core column are plump and present spindle-shape, without obvious pinch phenomenon, but with good seismic performance.

3) The longitudinal baffle of multi-core column can effectively restrain the outside deformation of steel plate plane so as to improve the buckling capacity of steel plate. The I-shaped cross section formed by the baffle and the column web provides effective restraint on the concrete so as to ensure that the members have sufficient vertical bearing capacity under horizontal reversed loading.

4) The multi-core column has good deformation ability, so when the axial compression ratio is designed as 0.54 to 0.68, the yield displacement angle is greater than 0.005rad, and the ultimate displacement angle is greater than 0.02rad. The displacement ductility coefficient of the specimens is greater than 3, and the equivalent damping viscosity coefficients are all greater than 0.4. Increasing the steel ratio of members can effectively increase the energy-dissipation capacity of specimens.

5) When the specimen reaches the peak load, the strain distribution at its the bottom section is in line with the plane cross-section assumption, and the horizontal ultimate bearing capacity obtained by the proposed formula in this paper is in good agreement with the experimental results.

Acknowledgement

National key research and development plan (2017YFC0703800)

Science and technology development plan of Shaanxi Provincial Construction Department (2016-K86)

References

[1] Hao Jiping,Sun Xiaoling, Xue Qiang, et al.: (2017) *Research and application of fabricated steel structure building system* [J]. Engineering Mechanics, 34(1): 1-13.

[2] Morino Shosuke: (2000). *Recent developments on concrete-filled steel tube members in Japan* [C]// Composite Construction in Steel and Concrete IV. Banff, Alberta, Canada: ASCE 2000: 644-655.

[3] Han Linhai, You Jingtuan, Yang Youfu, et al. (2004) *Behavior of concrete-filled steel rectangular hollow sectional columns subjected to cyclic loading* [J]. China Civil Engineering Journal, 37(11): 11-22.

[4] Huang Hong, Zhang Ange, Li Yi, et al: (2011) *Experimental research and finite element analysis on mechanical performance of concrete-filled stiffened square steel tubular stub columns subjected to axial compression*[J]. Journal of Building Structures, 32(2): 75-82.

[5] Cai Jian, Long Yueling: (2009) *Axial bearing capacity of square and rectangular CFT stub columns with binding bars*[J]. Journal of Building Structures, 30(1): 7-14.

[6] Guo Lanhui, Zhang Sumei, Xu Zheng, Et al.: (2011) *Experimental and theoretical analysis of stiffened rectangular composite columns with large height-to-breadth ratios* [J]. China Civil Engineering Journal, 44(1): 42-49.

[7] CECS 159:2004. *Technical specification for structures with concrete-filled rectangular steel tube members* [S]. Beijing: China Planning Press, 2004.

[8] ANSI/AISC 360-10. *Specification for Structural Steel Buildings* [S]. Chicago, Illinois USA: AISC, 2010.

[9] BS EN 1994-1-1:2004. *Eurocode 4: Design of composite steel and concrete structures* [S]. London UK: British Standard Institution, 2005.

[10] JGJ/T 101-2015 *Specification for seismic test of buildings* [S]. Beijing: China Architecture & Building Press, 2015.

[11] Han Linhai, Tao Zhong: (2000) *Ductility coefficient of concrete filled steel tubular columns with square sections* [J]. Journal of Earthquake Engineering and Engineering Vibration, 20(4): 56-65.

[12] GE HB, USAMI T: (1994) *Strength analysis of concrete-filled thin-walled steel box columns* [J]. Journal of Constructional Steel Research, 30 (3), 259-281.

[13] Mander JB, Priestley MJN, Park R: (1988) Theoretical stress-strain model for confined concrete[J]. Journal of Structural Engineering, ASCE, 114(8):1804–1826.

[14] Long Yueling, Cai Jian: (2013) *Stress–strain relationship of concrete confined by rectangular steel tubes with binding bars*[J]. Journal of Constructional Steel Research, 88:1–14.

[15] Pramono E, Willam K: (1989) *Fracture-energy based plasticity formulation of plain concrete*[J]. Journal of Engineering Mechanics, ASCE, 115(8):1183–1204.

[16] Xilin L U, Zhang G, Chen S: (2009) *Research on seismic behavior of full-scale high-strength concrete frame columns with high axial compression ratios*[J]. Journal of Building Structures, 30(3):20-26.

[17] Xu Y F, Song J, Sun P J: (2012) *Study on Seismic Behavior of T-shaped Concrete-filled Steel Tube Compound Column under Different Axial Compression Ratios*[J]. Advanced Materials Research, 368-373:1539-1542.

Received May 7, 2017